

Leptonic widths of heavy quarkonia: S-Wave QCD/NRQCD matching coefficients for the electromagnetic vector annihilation current at $\mathcal{O}(\alpha_s v^2)$

A. Hart,¹ G.M. von Hippel,² and R.R. Horgan³

¹*SUPA, School of Physics, University of Edinburgh, Edinburgh EH9 3JZ, United Kingdom*

²*Department of Physics, University of Regina, Regina, Saskatchewan S4S 0A2, Canada*

³*Department of Applied Mathematics and Theoretical Physics, University of Cambridge, Centre for Mathematical Sciences, Cambridge CB3 0WA, United Kingdom*

We construct the S-wave part of the electromagnetic vector annihilation current to $\mathcal{O}(\alpha_s v^2)$ on the lattice for heavy quarks whose dynamics are described by the NRQCD action, and v is the non-relativistic quark velocity inside the meson. The lattice vector current for $Q\bar{Q}$ annihilation is expressed as a linear combination of lattice operators with quantum numbers $L = 0, J^P = 1^-$, and the coefficients are determined by matching this lattice current to the corresponding continuum current in QCD to $\mathcal{O}(v^2)$ at one-loop. The annihilation channel gives a complex amplitude and a proper choice for the contours of integration is needed; a simple Wick rotation is not possible. In this way, and with a careful choice of subtraction functions in the numerical integration, the Coulomb-exchange and infrared singularities appearing in the amplitudes are successfully treated. The matching coefficients are given as a function of the heavy quark mass Ma in lattice units. An automated vertex generation program written in PYTHON is employed, allowing us to use a realistic NRQCD action and an improved gluon lattice action. A change in the definition of either action is easily accommodated in this procedure. The final result, when combined with lattice simulation results, describes the electromagnetic decays of heavy quarkonia, notably the Υ meson.

PACS numbers: 12.38.Bx, 12.38.Gc, 13.20.Gd

I. INTRODUCTION

Heavy quark states like the J/Ψ [1, 2] and Υ [3, 4] mesons play a central role in the experimental study of the electroweak interactions. It is therefore important that we have reliable non-perturbative QCD predictions of their properties against which to compare. Lattice Monte Carlo simulations provide the only systematically improvable framework for such studies, but relativistic quark actions do not lend themselves very easily to lattice simulations of heavy quark dynamics; the Compton wavelengths of heavy quarks are small compared to currently feasible lattice spacings.

Fortunately the heavy quarks are much heavier than the hadronic scale $\Lambda \approx 200$ MeV, whilst their kinetic energy is small (as demonstrated by the radial excitations of the mesons being much smaller than the ground state energy). This allows a non-relativistic description of the mesons using the NRQCD effective field theory [5, 6], using the heavy quark velocity as the expansion parameter.

Simply put, the goal of this paper is to provide matching coefficients that allow NRQCD matrix elements (calculated non-perturbatively in a lattice simulation) to be used to predict heavy quark phenomenology, in particular the leptonic widths of the Υ mesons.

More precisely, to obtain accurate results from a lattice simulation the QCD and NRQCD actions must be systematically improved to eliminate errors due to lattice artifacts, relativistic corrections and radiative effects. Both perturbative and non-perturbative methods exist to do this. A similar programme is needed for improvement of lattice operators and currents. In this paper we use perturbation theory to match matrix elements of the S-

wave part of the vector $Q\bar{Q}$ heavy-heavy electromagnetic annihilation current calculated on the lattice to the continuum result, ensuring that the lattice results give the correct answer to $\mathcal{O}(\alpha_s)$ in the strong coupling constant and $\mathcal{O}(v^2)$ in the velocity. This technique has already been used to improve the weak annihilation current for leptonic B-meson decay [7, 8] via the weak annihilation of a heavy quark Q and light anti-quark \bar{q} .

The $Q\bar{Q}$ annihilation is more complicated than the weak $Q\bar{q}$ case. In the heavy-light case, we can exploit the crossing symmetry of the relativistic light quark action to match instead the weak heavy-light Qq form-factor. The amplitude for this is purely real and so the choice of integration contour for the temporal component of the momentum is straightforward (parallel to the imaginary axis). The NRQCD action lacks this crossing symmetry and so the time-like improved lattice vector current (relevant for annihilation) is not *a priori* related to its space-like counterpart (which determines the heavy quark form-factor). The amplitude for on-shell $Q\bar{Q}$ annihilation is complex with a threshold for $Q\bar{Q}$ scattering and has the additional complication that it contains a Coulomb singularity. The calculation therefore entails a careful choice for the integration contours. For heavy quark velocities $v > 0$ this does not correspond to the simple Wick rotation (generally with constant real part displacement) which suffices for the improvement of the form-factor.

In addition, the Coulomb singularity gives rise to terms odd in v starting at $\mathcal{O}(v^{-1})$, and the integrand must be subtracted in a suitable way so that the numerical integral along the contour that passes close to the singularity can be done accurately. None of these difficulties occur in the matching calculations for the space-like weak and

electromagnetic form factors involving heavy quarks. We choose to match the real part of a suitable linear combination of the electromagnetic form-factors $F_1(q^2)$, $F_2(q^2)$ for time-like q with $q^2 = 4M^2(1 + v^2)$.

Earlier matchings of the vector annihilation current avoided these issues by either being restricted to tree level [9] or to $v = 0$ [10, 11]. Neither is satisfactory: v^2 and α_s are comparable at around 0.1 in the Υ system and failure to include both leads to strong discretisation errors in calculations of the leptonic width [12]. In addition, in [11] only the simplest NRQCD action was used, keeping only terms to leading order in v .

This study corrects this, using a gauge action that allows lattice matrix elements to be calculated using the state-of-the-art lattice QCD ensembles produced by the MILC collaboration. The NRQCD action is the same improved form used in recent studies, e.g. [12, 13]. When the matching coefficients calculated here are married to lattice NRQCD matrix elements, it will allow a determination of the leptonic width that is correct to $\mathcal{O}(10\%)$ and of the ratio of the widths of the 2S and 1S Υ states correct to within a few per cent. The size of these uncertainties matches those in the experimental measurements [12], which justifies our one-loop, perturbative approach in the matching.

The structure of the paper is as follows. In Sec. II we describe the matching procedure. The continuum QCD matrix element analytic calculation is given in Sec. III. In Sec. IV we present the numerical calculation of the corresponding NRQCD matrix elements. The final matching coefficients are determined in Sec. V, and discussed in Sec. VI. In the appendices, we describe the tests we have applied in our calculation to ensure the correctness of the Feynman rules and of the loop integration, and also to establish the independence of the results on the gauge fixing and infrared regulator.

A preliminary version of this work was presented in Ref. [14].

II. MATCHING S-WAVE DECAYS

The leptonic width of a heavy quarkonium state of mass $M_{\bar{Q}Q}$ is given in terms of a QCD matrix element M_{ME} by

$$\Gamma_{ee} = \frac{16\pi}{6M_{\bar{Q}Q}^2} |M_{\text{ME}}|^2 e_Q^2 \alpha_{\text{em}}^2 \quad (1)$$

where e_Q is the electric charge of the heavy quark and α_{em} the fine structure constant. The matrix element represents the probability of the heavy quarks meeting and annihilating, and in the simplest picture is represented by a hydrogenic ‘‘wavefunction at the origin’’: $|M_{\text{ME}}|^2 \simeq \psi^\dagger \psi(0)$.

To compare with the experimentally measured widths, we want to calculate this matrix element in continuum QCD, in a way that embodies all the non-perturbative

dynamics. As explained in the introduction, we cannot do this directly and must instead use lattice NRQCD simulations.

The problem is that we do not know a priori which NRQCD current we should use. Instead, we should consider a set of suitable currents and separately calculate the matrix elements of each one using the Monte Carlo generated ensemble. The true QCD matrix element is a linear combination of these, and this paper provides the necessary coefficients.

We choose our NRQCD currents to be

$$\mathbf{J}_i = \boldsymbol{\sigma} \left(\frac{\Delta^2}{M^2} \right)^i \quad (2)$$

where bold face symbols denote spatial 3-vectors and M is the heavy quark mass.

To convert our non-perturbative lattice NRQCD current matrix elements into the corresponding QCD value, $M_{\text{ME}} = \langle 0 | J^{\text{QCD}} | \bar{Q}Q \rangle$, we need matching coefficients a_i such that

$$\langle 0 | \mathbf{J}^{\text{QCD}} | \bar{Q}Q \rangle = \sum_i a_i \langle 0 | \mathbf{J}_i | \bar{Q}Q \rangle . \quad (3)$$

In this paper we fix them.

When we calculate the matrix elements of J_i in the simulation, the mass M will of course be replaced by a number. We may choose it to be the bare mass or (less usually) the renormalised value. The a_i will differ accordingly, so we will give separate results for the bare and renormalised cases.

Our matching method is summarised as follows: the NRQCD matrix elements each depend differently on the heavy quark velocity (at tree level, for instance, $\langle 0 | J_i | \bar{Q}Q \rangle \propto v^{2i}$). By choosing the a_i appropriately we can match the QCD velocity dependence order by order in v^2 . We make this choice perturbatively, performing the velocity matching at each order in α_s in turn [15].

We start by expanding the currents and matching coefficients as power series in α_s :

$$a_i = \sum_n \alpha_s^n a_i^{(n)} , \quad \langle 0 | \mathbf{J} | \bar{Q}Q \rangle = \sum_n \alpha_s^n \langle 0 | \mathbf{J} | \bar{Q}Q \rangle^{(n)} . \quad (4)$$

The superscript (n) denotes the $\mathcal{O}(\alpha_s^n)$ perturbative contribution.

Working in the Breit frame (where the decaying meson is stationary), we take the Euclidean four momentum of the quark and antiquark to be

$$p^\mu = (iE_0, \pm \mathbf{p}) , \quad \mathbf{p} = (0, 0, aMv) . \quad (5)$$

The dimensionless expansion parameter is v . Although we refer to it as the heavy quark velocity, it is related to the true velocity by $v = \beta / \sqrt{1 - \beta^2}$.

We treat the heavy quarks as being on shell. This is exact, even though we might expect off shell contributions at $\mathcal{O}(\alpha_s^2)$. By using the equations of motion, the contributions from these within a bound state are seen to vanish at all but a subset of spacetime points of measure zero [16, 17].

A. Matching at tree level

The matching at tree level is essentially trivial. Using the standard Dirac representation for the γ -matrices in terms of Pauli σ -matrices:

$$\gamma^0 = \begin{pmatrix} 1 & 0 \\ 0 & -1 \end{pmatrix}, \quad \gamma^i = \begin{pmatrix} 0 & \sigma^i \\ -\sigma^i & 0 \end{pmatrix}, \quad (6)$$

the spinors become

$$u(\mathbf{p}) = \begin{pmatrix} \psi \\ \frac{\boldsymbol{\sigma} \cdot \mathbf{p}}{E+M} \psi \end{pmatrix} \sqrt{\frac{E+M}{2E}},$$

$$v(\mathbf{p}) = \begin{pmatrix} \frac{\boldsymbol{\sigma} \cdot \mathbf{p}}{E+M} \chi \\ \chi \end{pmatrix} \sqrt{\frac{E+M}{2E}}, \quad (7)$$

where ψ and χ are the standard Pauli spinors for quarks and antiquarks, respectively. We have chosen the non-relativistic normalisation for consistency with NRQCD, since the Foldy-Wouthuysen-Tani transformation [18, 19, 20, 21] is unitary.

In terms of these Pauli spinors, the relevant Dirac tensor components of the non-relativistic expansion of the tree-level matrix element $\langle 0 | J^{\text{QCD};\mu} | \bar{Q}Q \rangle^{(0)} \equiv \bar{v}(-\mathbf{p})\gamma^\mu u(\mathbf{p})$ are:

$$\begin{aligned} \bar{v}(-\mathbf{p})\gamma^0 u(\mathbf{p}) &= 0, \\ \bar{v}(-\mathbf{p})\gamma u(\mathbf{p}) &= \chi^\dagger \boldsymbol{\sigma} \left(\frac{2}{3} + \frac{M}{3E} \right) \psi \\ &\equiv f_1(v^2) \chi^\dagger \boldsymbol{\sigma} \psi, \\ \bar{v}(-\mathbf{p})\frac{i\sigma^{i0}E}{M} u(\mathbf{p}) &= \chi^\dagger \sigma^i \left(\frac{E}{3M} + \frac{2}{3} \right) \psi \\ &\equiv f_2(v^2) \chi^\dagger \sigma^i \psi. \end{aligned} \quad (8)$$

where we have averaged over spatial directions for S-wave decays [9].

The tree-level matching coefficients must satisfy the leading order term in Eq. (3):

$$\langle 0 | \mathbf{J}^{\text{QCD}} | \bar{Q}Q \rangle^{(0)} = \sum_i a_i^{(0)} \langle 0 | \mathbf{J}_i | \bar{Q}Q \rangle^{(0)} \quad (9)$$

The expansions in powers of v are

$$f_1(v^2) = 1 - \frac{1}{6}v^2 + \frac{1}{8}v^4 + \mathcal{O}(v^6),$$

$$f_2(v^2) = 1 + \frac{1}{6}v^2 - \frac{1}{24}v^4 + \mathcal{O}(v^6). \quad (10)$$

Using Eq. (5), the tree level NRQCD matrix elements can be written as

$$\langle 0 | \mathbf{J}_i | \bar{Q}Q \rangle^{(0)} = g_i(v) \chi^\dagger \boldsymbol{\sigma} \psi. \quad (11)$$

The tree level velocity dependence is

$$g_0(v) = 1$$

$$g_1(v) = -\frac{4}{(aM)^2} \sin^2 \left(\frac{aMv}{2} \right)$$

$$g_2(v) = \frac{4}{(aM)^4} \left[4 \sin^2 \left(\frac{aMv}{2} \right) - \sin^2(aMv) \right] \quad (12)$$

such that $g_i(v) = (-v^2)^i$ at lowest order in v .

A term by term comparison of these expansions with that of f_1 yields

$$a_0^{(0)} = 1, \quad a_1^{(0)} = \frac{1}{6}, \quad a_2^{(0)} = \frac{1}{8} - \frac{(aM)^2}{72}. \quad (13)$$

B. Matching at one-loop order

To match at one-loop order, we need to calculate the one-loop QCD and NRQCD corrections to the quark-antiquark annihilation vertex. The QCD corrections consist of both self-energy insertions on the external legs and a vertex correction, and for the case of a quark-antiquark vertex can be written as

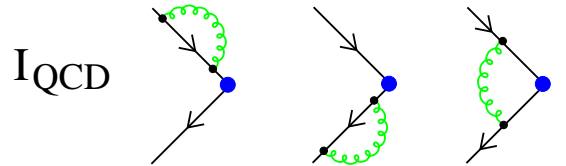


FIG. 1: One-loop corrections to the quark-antiquark annihilation current in QCD

$$\begin{aligned} \langle 0 | \mathbf{J}^{\text{QCD}} | \bar{Q}Q \rangle^{(1)} &= F_1^{(1)}(4E^2) \bar{v}(-\mathbf{p})\boldsymbol{\gamma}u(\mathbf{p}) + iF_2^{(1)}(4E^2) \bar{v}(-\mathbf{p})\tilde{\mathbf{q}}u(\mathbf{p}) \\ &= \left[F_1^{(1)}(4E^2)f_1(v^2) + F_2^{(1)}(4E^2)f_2(v^2) \right] \chi^\dagger \boldsymbol{\sigma} \psi \end{aligned} \quad (14)$$

where $\tilde{q}_i \equiv \sigma_{i\nu} q^\nu / M$ and $F_{1,2}^{(1)}$ are the $\mathcal{O}(\alpha_s)$ contributions to the vertex structure functions. We note that while after renormalisation $F_1^{(1)}$ is UV-finite because of the Ward identity, it contains IR divergences. These infrared divergences, however, are the same as those that arise in NRQCD, since the low-energy behaviour of the two theories is the same.

The $\mathcal{O}(\alpha_s)$ matching condition from Eq. (3) is then

$$\begin{aligned} \sum_i a_i^{(1)} \langle 0 | \mathbf{J}_i | \bar{Q}Q \rangle^{(0)} &= \left[F_1^{(1)}(4E^2) f_1(v^2) + F_2^{(1)}(4E^2) f_2(v^2) \right] \chi^\dagger \boldsymbol{\sigma} \psi - \sum_i a_i^{(0)} \langle 0 | \mathbf{J}_i | \bar{Q}Q \rangle^{(1)} \\ &\equiv (I_{\text{QCD}} - I_{\text{NRQCD}}) \chi^\dagger \boldsymbol{\sigma} \psi \end{aligned} \quad (15)$$

The infrared divergences cancel between the first two terms, leaving an IR- and UV-finite expression that can be evaluated numerically. We opt to project out the σ_2 component and use the tree-level expectation values of the NRQCD operators J_i as our basis functions to fit the difference between the QCD and NRQCD one-loop results and determine $a_i^{(1)}$:

$$\sum_i a_i^{(1)} g_i(v) = I_{\text{QCD}} - I_{\text{NRQCD}}. \quad (16)$$

To match to $\mathcal{O}(v^2)$ in this calculation i runs from 0 to 1 only.

III. CONTINUUM QCD CALCULATION

To evaluate I_{QCD} analytically, we must regulate the infrared Coulomb divergence in the Feynman integrals. To avoid the complications of twisted boundary conditions, we introduce a gluon mass μ and use the gauge invariant Stückelberg propagator for the massive vector field (see Sec. (3-2-3) of Ref. [22]):

$$G_{\mu\nu} = \frac{g_{\mu\nu} - k_\mu k_\nu / \mu^2}{k^2 - \mu^2 + i\varepsilon} + \frac{k_\mu k_\nu / \mu^2}{k^2 - \mu^2 / \lambda + i\varepsilon} \quad (17)$$

where λ is the gauge fixing parameter.

The one-loop QCD contribution is given by the sum of the Feynman diagrams shown in Fig. 1. The two leftmost rescale the tree-level element by the quark wave function renormalisation constant Z . The rightmost diagram is the one-loop vertex correction. The full one-loop vertex function is a rather formidable-looking expression [23]. We know from the Ward identity, however, that the vertex function must take the form

$$\bar{u}(\mathbf{p}') \Gamma_\mu u(\mathbf{p}) = \bar{u}(\mathbf{p}') \left[F_1(q^2) \gamma_\mu + \frac{i}{2M} F_2(q^2) \sigma_{\mu\nu} q^\nu \right] u(\mathbf{p}) \quad (18)$$

when sandwiched between on-shell spinors, where $q = p - p'$ is the gluon momentum flowing out of the vertex. We also know from the Ward identity that $Z^{-1} = F_1(0)$, so that we can renormalise the vertex function order by order by subtracting from $F_1(q^2)$ its value at zero gluon momentum to obtain the renormalised structure function

$$F_1^{(n),R}(q^2) = F_1^{(n)}(q^2) - F_1^{(n)}(0). \quad (19)$$

This amounts to including the effects of the first two diagrams, with which we will therefore no longer concern ourselves.

For the case of quark-antiquark annihilation, we then have

$$\langle 0 | J_\mu^{\text{QCD}} | \bar{Q}Q \rangle^{(1)} = \bar{v}(-\mathbf{p}) \left[F_1^{(1),R}(4E^2) \gamma_\mu + \frac{iE}{M} F_2^{(1)}(4E^2) \sigma_{\mu 0} \right] u(\mathbf{p}) \quad (20)$$

or, in terms of Pauli spinors

$$\langle 0 | J_i^{\text{QCD}} | \bar{Q}Q \rangle^{(1)} = \chi^\dagger \sigma_i \psi \left[F_1^{(1),R}(4E^2) f_1(v^2) + F_2^{(1)}(4E^2) f_2(v^2) \right]. \quad (21)$$

To compute F_1 and F_2 without resorting to the Feynman or Schwinger parameter representations (which are not available for NRQCD because the denominators are not quadratic), we employ a number of techniques. A discussion of these will be useful later.

Since the decomposition of the vertex function into form factors stated above is only valid between on-shell spinors, we put it between the appropriate on-shell projectors

$$(\not{p}' + M)\Gamma_\mu(p', p)(\not{p} + M) = (\not{p}' + M) \left[F_1(q^2)\gamma_\mu + \frac{i}{2M}F_2(q^2)\sigma_{\mu\nu}q^\nu \right] (\not{p} + M) \quad (22)$$

where the appropriate on-shell momenta for an incoming quark-antiquark pair are given by $p_\mu = (E, \mathbf{p})$ and $p'_\mu = (-E, \mathbf{p})$ with $E = \sqrt{M^2 + \mathbf{p}^2}$.

Contracting the above equation with either $(p + p')^\mu$ or γ^μ , and taking the trace of both sides, we obtain two equations for F_1 and F_2 :

$$\begin{aligned} A &\equiv \frac{(p + p')^\mu}{2M} \text{Tr}((\not{p}' + M)\Gamma_\mu(p', p)(\not{p} + M)) \\ &= \frac{(p + p')^2}{2M^2} (4M^2 F_1(q^2) - q^2 F_2(q^2)), \\ B &\equiv \text{Tr}(\gamma^\mu (\not{p}' + M)\Gamma_\mu(p', p)(\not{p} + M)) \\ &= 4(2M^2 + q^2)F_1(q^2) - 6q^2 F_2(q^2), \end{aligned} \quad (23)$$

with solutions

$$\begin{aligned} F_1(q^2) &= \frac{1}{4(4M^2 - q^2)} \left[\frac{12M^2}{(p + p')^2} A - B \right], \\ F_2(q^2) &= \frac{2M^2(2M^2 + q^2)}{q^2(p + p')^2} \\ &\quad \times \left[\frac{A}{(p + p')^2} - \frac{B}{2(2M^2 + q^2)} \right]. \end{aligned} \quad (24)$$

At the one-loop level, the vertex function is given by the integral expression (in Feynman gauge)

$$\Gamma_\mu^{(1)}(p', p) = 4\pi C_2 \int \frac{d^4 k}{(2\pi)^4} \frac{\gamma_\rho (\not{l}' + M)\gamma_\mu (\not{l} + M)\gamma^\rho}{(k^2 - \mu^2)(l'^2 - M^2)(l^2 - M^2)} \quad (25)$$

where we have defined the loop momenta $l = k + p$ and $l' = k + p'$ and introduced a gluon mass μ as an infrared regulator. After performing the manipulations outlined above, this vertex function leads to

$$\begin{aligned} F_1^{(1)}(q^2) &= 4\pi C_2 \int \frac{d^4 k}{(2\pi)^4} \frac{4}{(p + p')^2(k^2 - \mu^2)(l'^2 - M^2)(l^2 - M^2)} \\ &\quad \times \left[2M^2 l \cdot l' + 2M^2(p + p') \cdot (l + l') - \frac{6M^2}{(p + p')^2}(p + p') \cdot l (p + p') \cdot l' \right. \\ &\quad \left. + 2p \cdot l' p' \cdot l - M^4 - M^2 p \cdot p' \right], \\ F_2^{(1)}(q^2) &= 4\pi C_2 \int \frac{d^4 k}{(2\pi)^4} \frac{2M^2(2M^2 + q^2)}{q^2(p + p')^2(k^2 - \mu^2)(l'^2 - M^2)(l^2 - M^2)} \\ &\quad \times \left[4((p + p') \cdot (l + l') + l \cdot l' - M^2) - \frac{2}{(p + p')^2}(p + p') \cdot l (p + p') \cdot l' \right. \\ &\quad \left. - \frac{8}{2M^2 + q^2} (M^2 l \cdot l' - 2p \cdot l' p' \cdot l + M^2(p + p') \cdot (l + l') + p \cdot p' - 2M^2) \right] \end{aligned} \quad (26)$$

for the structure functions.

In the physical limit $\mu \rightarrow 0$, the one-loop structure functions are of course well-known analytically, since they are just the QED structure functions multiplied by the

group-theoretic factor $C_2 = 4/3$:

$$\begin{aligned} F_1^{(1),R}(q^2) &= \frac{g^2 C_2}{4\pi^2} \left[\left(\log \frac{\mu}{M} + 1 \right) (\theta \cot \theta - 1) \right. \\ &\quad \left. + 2 \cot \theta \int_0^{\theta/2} \phi \tan \phi d\phi + \frac{\theta}{4} \tan \frac{\theta}{2} \right] \\ F_2^{(1)}(q^2) &= \frac{g^2 C_2}{8\pi^2} \frac{\theta}{\sin \theta} \end{aligned} \quad (27)$$

where

$$\theta = 2 \arcsin(E/M) \quad (28)$$

We have compared our numerical evaluation of the structure functions in both the form factor and annihilation channels with their analytical values and have found excellent agreement. Especially, we were able to replicate the infrared divergence by varying our gluon mass μ . Resolving the $1/v$ Coulomb singularity in the annihilation channel requires special care. To avoid a contamination of the low- v behaviour by the gluon mass μ , which acts as a cut-off on the v dependence by limiting the momentum of the exchanged gluon, we have scaled μ with v , and then were able to observe the correct Coulomb singularity behaviour in the infrared finite part of F_1 .

A. Wick rotation

In doing these calculations, we must be careful how we Wick rotate our integration contour. In the quark-antiquark annihilation channel, the poles of the integrands in the complex k_0 plane are located as shown in Fig. 2. For $(\mathbf{k} + \mathbf{p})^2 > \mathbf{p}^2$, the poles are all located second and fourth quadrants of the Argand diagram for k_0 , and the usual Wick rotation of the integration contour is possible as in Fig. 2a. When $(\mathbf{k} + \mathbf{p})^2 \leq \mathbf{p}^2$, the fermionic poles cross the imaginary k_0 axis and we need to be more careful and deform the contour as per Fig. 2b. This choice of contour is, however, impractical. The short piece of the contour running along the real axis is by far the most dominant contribution to the integral. We will estimate the value of the integral using Monte Carlo methods. To get this contribution correctly, we need to sample all three-momenta along the contour with comparable weights. We therefore use the equivalent contour shown in Fig. 2c, which works much more efficiently.

In this triple contour case, we choose the outlying contours to be midway between the gluonic and fermionic poles. The Stückelberg gluon propagator has two poles: one associated with the physical gluon mass, and a second at μ^2/λ . To avoid possible numerical instabilities, we use the smaller of the two to fix the position of the outer two contours.

Note that if we work with $v = 0$ as in Ref. [10] we can always Wick rotate as per Fig. 2a. For non-zero v , however, it is important to note that the choice of an appropriate contour is essential to obtain the correct result: with a naive standard Wick-rotation, the structure functions obtained would not even be Lorentz-invariant. We have explicitly checked that our choice of contours leads to structure functions that are invariant under a Lorentz boost. Another point to note is that even in the quark form factor channel at spacelike q^2 , where the quark poles do not cross each other, a standard Wick rotation about the origin is not correct, and the rotated contour has to be shifted along the real axis by an amount depending on

the kinematic frame, in order to pass between the poles and pick up the correct result.

IV. LATTICE NRQCD CALCULATION

In this section we describe the perturbative calculation using the lattice NRQCD action.

1. The NRQCD Action

The NRQCD action we consider is the same as Gulez et al. [13], and also the same as has been used in recent simulations [12, 29] (although there is a typographical error in the description in the latter [24]):

$$\begin{aligned} \mathcal{S}_{\text{NRQCD}} = & \sum_{x,t} \psi^\dagger \psi - \psi^\dagger \left(1 - \frac{a\delta H}{2}\right) \left(1 - \frac{aH_0}{2n}\right)^n \\ & \times U_4^\dagger \left(1 - \frac{aH_0}{2n}\right)^n \left(1 - \frac{a\delta H}{2}\right) \psi, \quad (29) \end{aligned}$$

The ψ^\dagger field is understood to be located at (t, \mathbf{x}) , with the position of ψ on the timeslice $t - 1$ fixed by gauge invariance. Other than consistency with previous work, there are no strong arguments for the relative ordering of the kinetic and interaction terms in the action. The ordering here differs from, for instance, Ref. [6].

The leading kinetic term is

$$H_0 = -\frac{\Delta^2}{2aM} \quad (30)$$

where M is the bare mass and n is a stability parameter for the nonrelativistic evolution equation, that must fulfil the condition $n > 3/(2aM)$ for the time reversal symmetric evolution equation [6, 25]. Gluonic corrections decrease the lower bound on n to just above $1/(aM)$ [26].

The time-reversal symmetric splitting of the H_0 operator either side of the temporal link [6] is designed to mimic the full time evolution due to H_0 along a temporal lattice spacing in a way that avoids the well-known instability in the discretisation of parabolic differential equations (see, for instance, Sec. 19.2 of Ref. [27]). In this way, the time step in the evolution equation is small enough to allow the highest momentum modes in the theory to come into equilibrium, whilst avoiding the need for a very small lattice spacing which makes the theory too expensive to simulate.

The interaction term corrects for relativistic and dis-

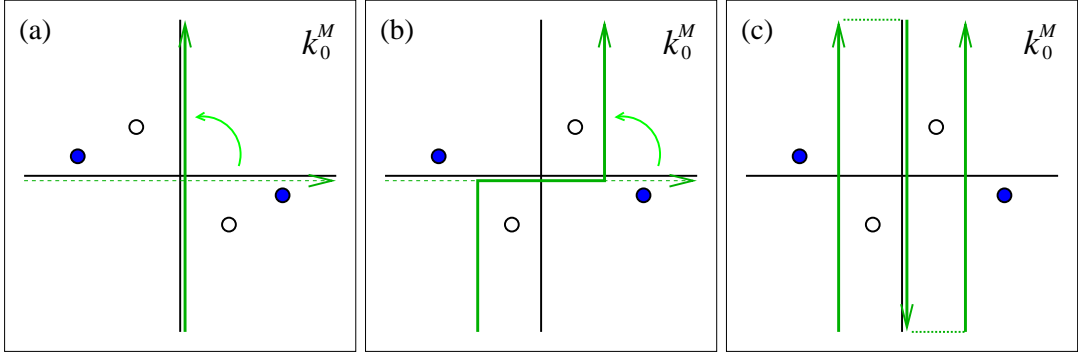


FIG. 2: Locations of the poles and choice of integration contour for the (Minkowski metric) k_0 integration in QCD quark-antiquark annihilation. The solid circles represent poles in the gluon propagator, and the open circles the fermionic poles for various $|\mathbf{k}|$.

cretisation effects:

$$\begin{aligned}
 a\delta H = & -c_1 \frac{(\Delta^{(2)})^2}{8(aM)^3} + c_2 \frac{i}{8(aM)^2} (\nabla \cdot \tilde{\mathbf{E}} - \tilde{\mathbf{E}} \cdot \nabla) \\
 & -c_3 \frac{1}{8(aM)^2} \boldsymbol{\sigma} \cdot (\tilde{\nabla} \times \tilde{\mathbf{E}} - \tilde{\mathbf{E}} \times \tilde{\nabla}) \\
 & -c_4 \frac{1}{2(aM)} \boldsymbol{\sigma} \cdot \tilde{\mathbf{B}} \\
 & +c_5 \frac{\Delta^{(4)}}{24(aM)} - c_6 \frac{(\Delta^{(2)})^2}{16n(aM)^2}. \quad (31)
 \end{aligned}$$

We note that improved derivatives are used in the term proportional to c_3 and that the improved field strength

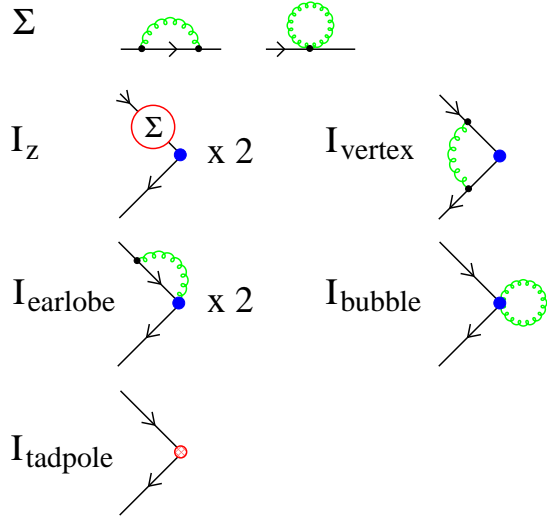


FIG. 3: One-loop corrections to the self energy and annihilation current in NRQCD. The gluons in these diagrams can be temporal as well as spatial. The solid (blue) circles represent the current in Eq. (3). The open (red) circle represents the contribution from tadpole improvement of the current. “ $\times 2$ ” denotes a similar diagram on the outgoing fermion line.

has not been rendered explicitly traceless. The terms proportional to c_i for $i = 1 \dots 4$ provide relativistic corrections to $\mathcal{O}(Mv^4)$ [6, 28] and represent the relativistic correction to the kinetic energy, the nonabelian analogue of the Darwin term, the spin-dependent interactions leading to spin-orbit couplings and the quark chromomagnetic moment, respectively. The final two terms remove the leading order discretisation error. All terms are understood to be tadpole improved. We use the tree level values $c_i = 1$, as in Refs. [12, 13]. Other than tadpole improvement, we do not consider the effects of radiatively correcting the c_i .

We obtain the Feynman rules for the NRQCD and gauge actions using an automated procedure [30], as outlined in Appendix A. We also detail there the tests we have carried out to ensure that the Feynman rule expressions are correct, and the techniques we employ to speed up their evaluation for specific momenta.

2. The lattice gauge action

To maintain compatibility with the MILC collaboration simulations, we use the Symanzik improved gauge action

$$\begin{aligned}
 S_G = & -\beta \sum_x \left(\frac{5}{3} P_{\mu\nu}(x) - \frac{1}{12} R_{\mu\nu}(x) - \frac{1}{12} R_{\nu\mu}(x) \right) \\
 & + \mathcal{O}(\alpha_s), \quad (32)
 \end{aligned}$$

where P, R are 1×1 and 2×1 Wilson loops respectively. $\mathcal{O}(\alpha_s)$ denotes possible radiative and tadpole improvement of the action. As discussed later, these terms will not contribute at one-loop.

The inverse lattice Stückelberg propagator is

$$\Gamma^{\mu\nu}(k) = V^{\mu\nu}(k) + (a\mu)^2 \delta^{\mu\nu} + \lambda \hat{k}^\mu \hat{k}^\nu, \quad (33)$$

where the two-point function $V^{\mu\nu}$ depends on the action chosen. Gauge invariance requires the gauge fixing term

TABLE I: Diagrams contributing to matching calculation. Where no statistical error is given, it is smaller than the quoted precision of the number.

aM	v	$(I_{\text{QCD}} - I_{\text{odd}})$	$(I_{\text{vertex}} - I_{\text{in}})$	I_{out}	I_Z	I_{earlobe}	I_{bubble}	I_{tadpole}	$I_{\text{QCD}} - I_{\text{NRQCD}}$
4.0	0					0.02155 (1)	-0.06695 (3)	0.04688	
	0.03	-0.8511	-1.3258 (28)	1.2176 (5)	1.8226 (9)	0.0216	-0.0668	0.0468	-0.1315 (30)
	0.07	-0.8611	-1.3112 (39)	1.2262 (5)	1.8212 (9)	0.0220	-0.0661	0.0463	-0.1452 (40)
	0.10	-0.8738	-1.2979 (44)	1.2370 (5)	1.8247 (9)	0.0224	-0.0652	0.0456	-0.1615 (45)
	0.15	-0.9044	-1.2636 (55)	1.2623 (5)	1.8288 (9)	0.0234	-0.0631	0.0441	-0.2004 (56)
2.8	0					0.05203 (2)	-0.13678 (5)	0.09566	
	0.03	-0.8511	-1.3689 (21)	0.9240 (4)	1.6225 (9)	0.0521	-0.1365	0.0956	-0.1736 (23)
	0.07	-0.8611	-1.3678 (29)	0.9468 (4)	1.6241 (9)	0.0526	-0.1359	0.0951	-0.1809 (31)
	0.10	-0.8738	-1.3659 (33)	0.9550 (4)	1.6249 (8)	0.0532	-0.1349	0.0944	-0.1862 (35)
	0.15	-0.9044	-1.3622 (39)	0.9726 (4)	1.6266 (9)	0.0545	-0.1327	0.0929	-0.2007 (40)
1.95	0					0.12394 (3)	-0.28210 (6)	0.19724	
	0.03	-0.8511	-1.3636 (15)	0.7415 (2)	1.3505 (8)	0.1241	-0.2820 (1)	0.1971	-0.1356 (17)
	0.07	-0.8611	-1.3669 (23)	0.7459 (2)	1.3486 (9)	0.1246	-0.2812 (1)	0.1966	-0.1357 (24)
	0.10	-0.8738	-1.3734 (26)	0.7503 (2)	1.3503 (9)	0.1254	-0.2804 (1)	0.1960	-0.1379 (27)
	0.15	-0.9044	-1.3979 (84)	0.7634 (4)	1.3537 (14)	0.1271 (1)	-0.2780 (1)	0.1944	-0.1319 (86)
1.0	0					0.5093 (2)	-1.0720 (4)	0.75000	
	0.07	-0.8611	-1.3681 (13)	0.5004 (2)	0.4335 (10)	0.5103 (2)	-1.0713 (4)	0.7494	0.4040 (17)
	0.10	-0.8738	-1.3956 (16)	0.5034 (2)	0.4323 (10)	0.5110 (2)	-1.0701 (4)	0.7488	0.4044 (19)
	0.15	-0.9044	-1.4146 (18)	0.5127 (2)	0.4323 (10)	0.5132 (2)	-1.0676 (4)	0.7472	0.4005 (21)

to be constructed from lattice momentum vector $\hat{k}^\mu \equiv 2 \sin(ak^\mu/2)$, so the Feynman gauge ($\lambda = 1$) propagator is only diagonal for the Wilson gauge action (for which the gluon two-point function is $V^{\mu\nu} = \hat{k}_\rho \hat{k}^\rho \delta^{\mu\nu} - \hat{k}^\mu \hat{k}^\nu$). Note that $\lambda = 1/\alpha$ in the notation of Ref. [31]. As we do not consider Landau gauge here, the inverse propagator is directly invertible and we do not need to use an intermediate gauge.

3. Annihilation currents and radiative improvements

We use lattice NRQCD annihilation currents that are the naive discretisations of Eq. (2):

$$\begin{aligned}
\mathbf{J}_0 &= \sum_x \chi_x^\dagger \boldsymbol{\sigma} \psi_x, \\
\mathbf{J}_1 &= \sum_{x;i=1}^3 \chi_x^\dagger \frac{\boldsymbol{\sigma}}{(aM)^2} \\
&\quad \times \left(U_i(x) \psi_{x+i} + U_i^\dagger(x-i) \psi_{x-i} - 2\psi_x \right) \quad (34)
\end{aligned}$$

and the links in \mathbf{J}_1 are understood to be tadpole improved. Removing the mean field, ‘‘tadpole’’ contributions improves the convergence of lattice perturbation theory markedly [32]. Operationally, this is done by dividing every gauge link U in the action by a factor of u_0 . Common definitions for u_0 are that it is the mean link in Landau gauge or the fourth root of the mean plaquette. We use the former, expanding the link perturbatively as $u_0 \equiv 1 - \alpha_s u_0^{(2)} + \dots$ with $u_0^{(2)} = 0.750$ from Ref. [33] and as used Ref. [13].

Tadpole improvement of the NRQCD action does not contribute to our calculation, as the fermion wavefunction renormalisation has no tadpole correction for the time reversal symmetric form of the NRQCD action (the argument mirrors the mean field analysis in Ref. [6]). As discussed before, we do not consider any further radiative improvements of the NRQCD action.

Tadpole and other radiative improvements of the gauge action also do not contribute to the matching calculation. The leading order effect of these is an $\mathcal{O}(\alpha_s)$ insertion in the gluon propagator. As there are no external gluons in our calculation, such insertions will only contribute at two loops and above.

The only effect of tadpole improvement comes from the current \mathbf{J}_1 , and its contribution to I_{NRQCD} can be easily calculated:

$$\begin{aligned}
I_{\text{tadpole}} &= \frac{2u_0^{(2)} a_1^{(0)}}{(aM)^2} \sum_{i=1}^3 \cos p_i, \\
&= -u_0^{(2)} a_1^{(0)} \left(-\frac{6}{(aM)^2} + v^2 + \mathcal{O}(v^4) \right) \quad (35)
\end{aligned}$$

The only other possible source of radiative corrections comes from the mass used in Eq. (2) when we calculate the non-perturbative NRQCD matrix elements in the Monte Carlo lattice simulation. If the number M used in the simulation is the renormalised heavy quark mass, there is no further correction. If the number for the bare mass is used instead, the renormalised mass is $Z_M M$ and we should divide the matching coefficient a_i by $(Z_M)^{2i}$. In this study, that amounts to shifting $a_1^{(1)} \rightarrow a_1^{(1)} - 2a_1^{(0)} Z_M^{(1)}$. We calculate the multiplicative mass renormalisation factor in Appendix B, and will

present our results for the matching coefficients both with and without the shift.

A. Calculating the vertex corrections

The one-loop diagrams contributing to the quark-antiquark annihilation amplitude in NRQCD are shown in Fig. 3. The NRQCD k_0 integrals are around the unit circle in the $e^{ik_0 a}$ -plane. The quark poles sometimes cross the unit circle (just as they crossed the imaginary axis in the QCD integrals), so we scale the circle of integration to avoid them and adopt a similar triple-contour strategy: integrating along three appropriately scaled concentric circles when the poles cross each other, and along the unit circle otherwise.

The $g_i(v)$ are all even functions of v , but I_{QCD} and I_{NRQCD} both contain odd powers. We must assure ourselves that these exactly cancel in Eq. (15). The argument is that NRQCD is an effective theory of QCD which can be systematically improved to reproduce all features of QCD, including the odd powers. There are, however, no S-wave operators containing odd powers of v that we could use in the improvement. The odd powers must therefore cancel exactly in Eq. (15). This is not entirely surprising given that the odd powers arise from an even polynomial in v multiplied by the $1/v$ Coulomb IR divergence, and we know that NRQCD must reproduce the IR physics exactly. Nonetheless, it is worth examining the cancellation in more detail.

Consider the power-expansion of the QCD expression

$$F_1^{(1),R}(4E^2)f_1(v^2) + F_2^{(1)}(4E^2)f_2(v^2) \quad (36)$$

with $F_1^{(1),R}$ defined in Eq. (19). Using the analytic results given above, we see that both $f_1(v^2)$ and $f_2(v^2)$ contain only even powers of v . Any odd powers in the expansion must therefore come from $F_1^{(1),R}(4E^2)$ or $F_2^{(1)}(4E^2)$. The analytical evaluation of the structure functions shows us that $F_2^{(1)}(4E^2)$ contains odd powers in v only in its imaginary part, so the odd powers in the final answer must come from $F_1^{(1),R}(4E^2)$.

On the NRQCD side, we know that any odd powers in v must come from the quark pole giving rise to the Coulomb singularity, since the residues in the k_0 -plane of all other poles can be expanded in powers of v^2 . The odd powers therefore originate exclusively from integrals of the form

$$\int \frac{d^3k}{(2\pi)^3} \frac{(\mathbf{k}^2)^\alpha (\mathbf{p}^2)^\beta}{\mathbf{k}^2 (\mathbf{k}^2 + 2\mathbf{k} \cdot \mathbf{p} + i\epsilon)}. \quad (37)$$

A careful analysis of these shows that only those integrals with $\alpha = 0$ contribute to the real part, whereas the others (which are UV-divergent in the continuum) contribute only to the imaginary part. Since

$$\int \frac{d^3k}{(2\pi)^3} \frac{1}{\mathbf{k}^2 (\mathbf{k}^2 + 2\mathbf{k} \cdot \mathbf{p} + i\epsilon)} = \frac{1}{16|\mathbf{p}|} \quad (38)$$

the only odd powers of v in the NRQCD result will come from multiplying powers of \mathbf{p}^2 in the numerator with the Coulomb singularity. Expanding these, we find the same coefficients multiplying each odd power of v as in the above QCD result.

We note that to obtain correct results to order v^{2n} we have to use the correctly matched $\mathcal{O}(v^{2n})$ tree-level annihilation operator. We must also use $\mathcal{O}(v^{2n})$ quark-gluon vertices in the diagram involving spatial gluons and the $\mathcal{O}(v^{2n+2})$ quark propagator (the expansion of the latter around the Coulomb singularity pole gives an $\mathcal{O}(v^{2n})$ contribution).

In summary, then, matching at tree-level to $\mathcal{O}(v^{2p})$ guarantees the cancellation of the odd powers at one-loop level to $\mathcal{O}(v^{2p-1})$.

We will estimate the NRQCD loop integrals stochastically using the adaptive Monte Carlo package called VEGAS [34, 35] (see Sec. 7.8 of Ref. [27] for further discussion). These estimates of the NRQCD integrals will only converge if the integrands are both finite and relatively smooth. Both I_{QCD} and I_{NRQCD} have an infrared Coulomb divergence. Although these are formally regulated by the gluon mass, the integrands are still sharply peaked, leading to unacceptably slow convergence of the numerical integration.

As we have discussed, all odd powers of v cancel pointwise in the difference of the two integrands, $I_{\text{QCD}} - I_{\text{NRQCD}}$, leaving a smooth integrand. The obvious strategy is to numerically estimate the difference as a single integral, remembering that the NRQCD integrand is only defined inside the finite Brillouin zone.

Direct subtraction has problems. The NRQCD integrand is quite complicated and time-consuming to evaluate for given momenta. This limits the number of integration points that VEGAS can consider in a set time. Conversely, the QCD integrand needs a large number of points to accurately estimate the integral: the terms like $1/(p+p')^2$ in Eq. (26) give rise both to an apparently UV divergent contribution to the $1/v$ Coulomb singularity and $1/v^2$ term in the result. These terms, however, come with a factor of $\cos\theta$ from the scalar products with $(p+p')$, and thus vanish only after integration over all spatial angles.

If we directly subtract the integrands, we arrive at a function that is both expensive to evaluate and needs many integration points to converge. To get round this, we use an analytic form of the QCD structure functions and only evaluate the NRQCD integrals numerically. For the latter we need to smooth out the regulated $1/v$ infrared divergence by subtracting an integrand with the same low-momentum structure. Fortunately, we can still cancel all the odd powers of v from the NRQCD integrand by multiplying the integral to be subtracted by an

appropriate function of v^2 :

$$\begin{aligned}
I_{\text{odd}} &= \text{Im} \left\{ -\frac{4h(v^2)}{3} \int \frac{d^4k}{(2\pi)^4} (\mathbf{k}^2 + \mu^2)^{-1} \right. \\
&\quad \times \left(ik_0 - \frac{\mathbf{k}^2 + 2\mathbf{k} \cdot \mathbf{p}}{2M} \right)^{-1} \\
&\quad \times \left. \left(ik_0 + \frac{\mathbf{k}^2 + 2\mathbf{k} \cdot \mathbf{p}}{2M} \right)^{-1} \right\} \\
&= \frac{h(v^2)}{12v}
\end{aligned} \tag{39}$$

with

$$h(v^2) = \frac{(1 + 2v^2)(1 + 2\sqrt{1 + v^2})}{3(1 + v^2)}. \tag{40}$$

This is certainly sufficient for the low powers of v^2 in which we are interested here. By comparing the respective power-series expansions term by term, it can easily be seen that the odd powers of v are the same as in the QCD result.

To evaluate Eq. (16) we therefore take the difference of $(I_{\text{QCD}} - I_{\text{odd}})$ calculated analytically and $(I_{\text{NRQCD}} - I_{\text{odd}})$ estimated numerically. Both expressions are even power series in v , and the subtracted NRQCD integrand is now sufficiently smooth that no change of variable in the momentum coordinate, designed to “squash” many evaluation points onto the contour in the neighbourhood of the pole [36], is required. It is convenient to split I_{odd} into two integration regions, within (I_{in}) and outside (I_{out}) the NRQCD Brillouin zone $|k^\mu| \leq \pi/(aM)$.

I_{vertex} and I_{Z} separately have infrared “cutting” divergences that cancel in their sum. Although the divergences are regulated by the gluon mass, by evaluating I_{vertex} and I_{Z} together we would have a smoother integrand for VEGAS. We meet the same problem as before, however: I_{vertex} has a relatively cheap integrand but the VEGAS estimates are slow to converge. I_{Z} converges quickly, but taking derivatives of Feynman rules makes the integrand expensive to evaluate. Therefore, we calculate the NRQCD integrals in Fig. 3 separately using VEGAS, choosing the number of integration points to give comparable statistical accuracy in the results.

The final calculation is then made up of

$$\begin{aligned}
I_{\text{QCD}} - I_{\text{NRQCD}} &= (I_{\text{QCD}} - I_{\text{odd}}) - (I_{\text{NRQCD}} - I_{\text{odd}}) \\
&= (I_{\text{QCD}} - I_{\text{odd}}) - \\
&\quad ([I_{\text{vertex}} - I_{\text{in}}] - I_{\text{out}} + I_{\text{Z}} + I_{\text{earlobe}} \\
&\quad + I_{\text{bubble}} + I_{\text{tadpole}}).
\end{aligned} \tag{41}$$

V. RESULTS

In this paper we present results for four choices of heavy quark mass: $aM = 4.0, 2.8, 1.95$ and 1.0 . The

TABLE II: The matching coefficients, as a function of the renormalised heavy quark mass, for the leptonic width (a_i) and leptonic width ratio (b_i). Note that $a_0^0 = 1$, $a_1^0 = b_1^{(0)} = \frac{1}{6}$, and that there is *no* subtraction to prevent mixing down.

Ma	n	$a_0^{(1)}$	$a_1^{(1)}$	$b_1^{(1)}$	$b_2^{(0)}$
4.0	2	-0.1288 (27)	-3.29 (29)	-3.27 (30)	-0.09722
2.8	2	-0.1732 (21)	-1.27 (21)	-1.24 (22)	0.01611
1.95	2	-0.1358 (16)	-0.02 (16)	0.00 (17)	0.07219
1.0	4	0.4056 (20)	-0.22 (16)	-0.29 (17)	0.11111

TABLE III: The matching coefficients, as a function of the bare heavy quark mass, for the leptonic width (a_i) and leptonic width ratio (b_i). Note that $a_0^0 = 1$, $a_1^0 = b_1^{(0)} = \frac{1}{6}$, and that there is *no* subtraction to prevent mixing down.

Ma	n	$a_0^{(1)}$	$a_1^{(1)}$	$b_1^{(1)}$	$b_2^{(0)}$
4.0	2	-0.1288 (27)	-3.32 (29)	-3.30 (30)	-0.09722
2.8	2	-0.1732 (21)	-1.35 (22)	-1.32 (22)	0.01611
1.95	2	-0.1358 (16)	-0.16 (16)	-0.14 (17)	0.07219
1.0	4	0.4056 (20)	-0.50 (16)	-0.56 (17)	0.11111

first three represent the b -quark mass on the MILC improved staggered ensembles with $a \simeq 0.09$ fm (“fine”), 0.12 fm (“coarse”) and 0.17 fm (“super-coarse”) [12]. Mass $aM = 1$ represents the charm quark mass on the super-coarse lattices. In agreement with Ref. [12], we use $n = 2$ for all masses except $aM = 1.0$, where $n = 4$.

We choose IR gluon mass $(a\mu)^2 = 10^{-4}$ and use Feynman gauge $\lambda = 1$. In Appendix C we show that our results do not depend on either of these choices. We also compare with relevant existing results in the literature for $v = 0$.

The NRQCD diagrams were evaluated for a range of velocities from $v = 0.03$ to $v = 0.15$. In addition, we evaluated I_{bubble} and I_{earlobe} at $v = 0$. The results are shown in Table I. We extracted the matching parameters using a linear fit as per Eq. (16). The matching coefficients $a_0^{(1)}$ and $a_1^{(1)}$ are given in Tables II and III. Results from the former are to be used when the number for the renormalised heavy quark mass is used to construct the currents in Eq. (34). Results from the latter are to be used if the bare mass is instead employed.

The results in the renormalised mass case are shown graphically in Fig. 4. We note that for smaller masses, the coefficients of the J_1 current, $a_1^{(1)}$ and $b_1^{(1)}$, are much smaller when renormalised masses are used.

We have checked that the fits are not biased by higher terms in the velocity expansion. Note that whereas $-I_{\text{Z}}$, $-I_{\text{vertex}}$ and $-I_{\text{bubble}}$ reduce monotonically as aM is increased, I_{out} , $-I_{\text{earlobe}}$ and $-I_{\text{tadpole}}$ grow. Given that the result of combining these will depend on $(aM)^2$, $(aM)^4$ and $1/(aM)^2$, it is not surprising that the matching coefficients do not vary monotonically with the heavy quark mass.

Our computations of these diagrams have been per-

formed on the SunFire Galaxy-class supercomputer at the Cambridge-Cranfield High Performance Computing Facility using an implementation of the VEGAS algorithm adapted to parallel computers using MPI (Message Passing Interface).

A. Mixing downwards

Whilst at tree level matrix elements of J_1 contribute only at $\mathcal{O}(v^{2n})$, at higher loop orders there will be contributions at lower orders of v^2 . We call this “mixing down”. In the case of J_1 , the integrals I_{earlobe} , I_{bubble} and I_{tadpole} are only weakly momentum dependent and I_{vertex} also makes a contribution at $v = 0$.

This is theoretically inconvenient as we must redo all previous calculations when we improve the current to higher orders of v^2 and cannot easily compare the new numbers with the old to check for consistency. We can get around this by introducing subtracted currents to prevent this downward mixing of currents. Although not essential for lattice Monte Carlo calculations, subtracted currents are also useful here as they make the convergence of the double series in α_s and v^2 in Eqn. (3) most explicit. Thus we can expect that the matrix element of the subtracted J_1 will vary as v^2 (to some order in α_s).

We define the subtracted currents as $\bar{J}_i \equiv z_{ij} J_j$, where the coefficients z_{ij} are chosen to prevent this downward mixing of currents at all radiative orders:

$$\left| \langle 0 | \bar{J}_i | \bar{Q}Q \rangle^{(n)} \right| = v^{2i} + \mathcal{O}(v^{2(i+1)}) \quad \forall n. \quad (42)$$

At tree level $z_{ij}^{(0)} = \delta_{ij}$. At higher loop level we set $z_{ij}^{(n>0)} = 0$ for $j \geq i$, as we are only concerned with preventing downward mixing. For $\mathcal{O}(v^2)$ matching, the only non-trivial element is $z_{10}^{(1)}$, fixed by

$$\begin{aligned} z_{1j}^{(0)} \langle 0 | J_j | \bar{Q}Q \rangle^{(1)} + z_{1j}^{(1)} \langle 0 | J_j | \bar{Q}Q \rangle^{(0)} \Big|_{v=0} &= 0, \\ \Rightarrow z_{10}^{(1)} &= - \langle 0 | J_1 | \bar{Q}Q \rangle^{(1)} \Big|_{v=0}. \end{aligned} \quad (43)$$

Note that in this calculation we consider only I_{bubble} , I_{earlobe} , I_{tadpole} and I_{vertex} , all at $v = 0$. Data for $z_{10}^{(1)}$ are given in Table IV. The reader should note that the numbers in column 3 are not exactly the sum of the numbers for $v = 0$ in Table I. We have improved the accuracy of these by extrapolating data for all v to $v = 0$ using $g_1(v)$.

Correcting for mixing down does not change the tree level matching coefficients. The subtracted one loop factors are related to the original numbers by

$$\begin{aligned} \bar{a}_0^{(1)} &= a_0^{(1)} - z_{10}^{(1)}, \\ \bar{a}_1^{(1)} &= a_1^{(1)}. \end{aligned} \quad (44)$$

As this subtraction is less likely to be needed in a lattice evaluation of NRQCD matrix elements, it has *not* been applied to the results in Tables II and III.

TABLE IV: The mixing down subtraction. All diagrams are evaluated at $v = 0$. See the comment below Eqn. (43) for details of column 3.

Ma	n	$I_{\text{bubble}} + I_{\text{earlobe}} +$		
		I_{tadpole}	I_{vertex}	$z_{10}^{(1)}$
4.0	2	0.00146 (2)	-0.11889 (4)	0.11743 (5)
2.8	2	0.01094 (4)	-0.17265 (6)	0.16171 (8)
1.95	2	0.03907 (5)	-0.26196 (9)	0.22289 (11)
1.0	4	0.1870 (3)	-0.82970 (26)	0.6427 (4)

B. Matrix element ratios

If we are only interested in the ratio of leptonic widths of, say, $\Upsilon(2s)$ and $\Upsilon(1s)$, we do not care about the overall normalisation of the matrix element (which is independent of the mass of the meson). We can therefore express the ratio of leptonic widths as a ratio of differently normalised matrix elements

$$\begin{aligned} \frac{M_{\text{ME}}}{a_0} &= \langle J_0 \rangle + \frac{a_1}{a_0} \langle J_1 \rangle + \frac{a_2}{a_0} \langle J_2 \rangle \\ &\equiv \langle J_0 \rangle + b_1 \langle J_1 \rangle + b_2 \langle J_2 \rangle. \end{aligned} \quad (45)$$

The advantage of this is that for Υ states $v^2 \sim \alpha_s \sim 0.1$. We can obtain a *ratio* that is accurate to a few per cent, $\mathcal{O}(1\% - 5\%)$ (to two loops, effectively) by knowing a_0, a_1 to one loop and a_2 to tree level. That is, by knowing no more than we have already calculated in this paper:

$$\begin{aligned} b_1 &\equiv \frac{a_1}{a_0} = \frac{a_1^{(0)}}{a_0^{(0)}} + \frac{\alpha_s}{a_0^{(0)}} \left[a_1^{(1)} - \frac{a_1^{(0)} a_0^{(1)}}{a_0^{(0)}} \right], \\ b_2 &\equiv \frac{a_2}{a_0} = \frac{a_2^{(0)}}{a_0^{(0)}}. \end{aligned} \quad (46)$$

We give these values for the unsubtracted currents in Tables II and III. Note that the inclusion of J_2 at this order does not affect $a_0^{(1)}, a_1^{(1)}$, as there is no mixing down at tree level.

VI. SUMMARY AND CONCLUSIONS

In this paper we have presented a method to determine the QCD/NRQCD matching coefficients for electromagnetic decays of heavy quarkonia in lattice perturbation theory to order $\mathcal{O}(v^4, \alpha_s v^2)$. This calculation was carried out for a realistic lattice NRQCD action using largely automated methods for performing lattice perturbation theory.

The lattice NRQCD currents are given in Eq. (34). When calculating their matrix elements in a lattice Monte Carlo simulation, we have a choice as to whether we replace M by the renormalised heavy quark mass or the bare mass. If we choose M to be the renormalised heavy quark mass, the relevant matching coefficients are

given in Table II. If the bare mass is used instead, the matching coefficients include Z_M and are given in Table III.

We note that for the smaller quark masses, the $a_1^{(1)}$ and $b_1^{(1)}$ coefficients of the current J_1 are very much smaller when the renormalised quark mass is used. This is particularly relevant to NRQCD simulations of charm quarks on fine lattices, and shows that the use of the renormalised rather than bare mass is a major source of improvement in such simulations.

Individual Feynman diagrams vary monotonically with the mass, but when combined together the competing dependencies lead to the final answer varying as a complicated function of M .

We have performed a wide variety of checks of our calculation: we have confirmed that the Feynman rules are correctly generated by comparing with separately-obtained expressions in the literature, and that the one-loop self energy renormalisation similarly agrees. We have checked that the infrared divergences vary as expected with changes in the size of the regulating gluon mass and the choice of gauge. We have also checked that the final answer is independent of both of these factors. We have assured ourselves that the statistical errors quoted by VEGAS are consistent with the size of variations in the Monte Carlo estimates of the one-loop integrals.

These results could conceivably be checked using a series of high- β Monte Carlo simulations [37]. Looking further, the computation of the perturbative one-loop correction to the coefficient c_1 of the $\sigma \cdot \mathbf{B}$ could be carried out using the methods employed in this paper.

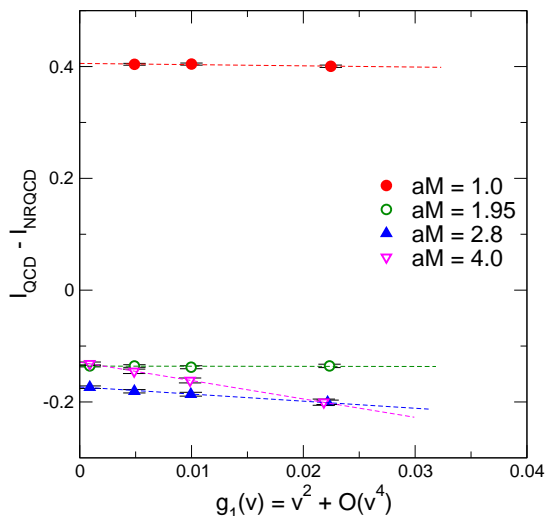


FIG. 4: The fits to the tadpole improved data versus velocity dependence of $\langle 0 | J_1 | \bar{Q} Q \rangle^{(0)}$.

Acknowledgments

The authors thank G.P. Lepage and C.T.H. Davies for useful discussions and the Cambridge–Cranfield High

Performance Computing Facility for advice and use of the SunFire supercomputer. A.H. thanks the U.K. Royal Society for financial support. The University of Edinburgh is supported in part by the Scottish Universities Physics Alliance (SUPA). G.M.v.H. is supported in part by the Canadian Natural Sciences and Engineering Research Council (NSERC) and by the Government of Saskatchewan.

APPENDIX A: FEYNMAN RULES

We use an automated method to obtain Feynman rules from the actions and currents used in this calculation. The algorithm and its implementation are described in Ref. [30]. This allows us to specify the action as a set of Wilson line contours that are then Taylor expanded. The symmetries of the action are exploited to produce very compact descriptions of the reduced vertex functions as sums of n monomials (each involving a relatively expensive exponentiation).

The gluonic action expansion has been tested in a number of calculations [31, 38, 39, 40]. The expansion of the currents was checked by hand.

We tested the NRQCD action expansion by comparing with the Feynman rules quoted in Eqs. (A11-A36) of Ref. [13]. We find complete agreement for general c_i , save in Eq. (A33) which gives the two gluon vertex for momenta specific to the gluon tadpole graph. Our automated method shows this expression to be incomplete; it should read:

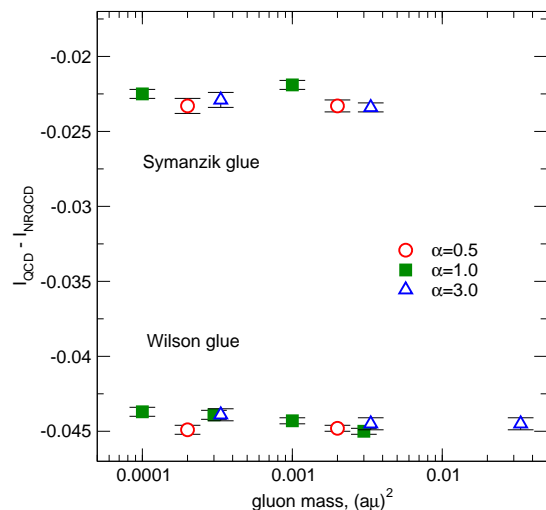


FIG. 5: $I_{\text{QCD}} - I_{\text{NRQCD}}$ for the NRQCD action described in Appendix C 2 at $aM = 2.1$ and $v = 0.03$.

$$\begin{aligned}
[O_1]_{s=0}^{(2)\mu,\nu}(k, k, q, -q) &= \left(\frac{c_1}{2(aM_0)^3} + \frac{c_6}{4n(aM_0)^2} \right) \delta_{\mu,i} \delta_{\nu,j} \left[\delta_{ij} \cos(k_j) \sum_{l=1}^3 \sin^2\left(\frac{k_l}{2}\right) + \frac{1}{2} \sin(k_i + \frac{q_i}{2}) \sin(k_j + \frac{q_j}{2}) \right] \\
&+ \frac{ic_2}{16(aM_0)^2} \left[(\delta_{\mu,j} \delta_{\nu,0} + \delta_{\mu,0} \delta_{\nu,j}) \cos(k_j + \frac{q_j}{2}) \sin(q_j) \cos(\frac{q_0}{2}) \eta_{j0} \right. \\
&\quad \left. - \delta_{\mu,j} \delta_{\nu,j} 2 \cos(k_j + \frac{q_j}{2}) \sin(q_0) \cos(\frac{q_j}{2}) \eta_{j0} \right] \\
&+ \frac{-c_5}{12(aM_0)} \delta_{\mu,j} \delta_{\nu,j} \left[\cos(k_j) - \cos(2k_j) \cos^2\left(\frac{q_j}{2}\right) + \frac{1}{2} \sin(2k_j) \sin(q_j) \right] \quad (A1)
\end{aligned}$$

where the change is the addition of the final, underlined term. This vanishes for $k = 0$ and so does not affect the results in Ref. [13]. Nonetheless, our detecting it highlights the usefulness of an automatic action expansion program both for developing new improved actions and for checking existing perturbative results. We are happy to share copies of the program with interested parties.

The NRQCD action in Eq. (29) naturally factorises into the product of several distinct operators:

$$S^{\text{NRQCD}} = \sum_t \psi_t^\dagger \psi_t - \psi_t^\dagger A_t B_t U_4^\dagger B_{t-1} A_{t-1} \psi_{t-1}, \quad (A2)$$

where

$$\begin{aligned}
A &= \left(1 - \frac{H_0}{2n} \right)^n, \\
B &= \left(1 - \frac{a\delta H}{2} \right), \quad (A3)
\end{aligned}$$

and the subscript refers to the timeslice on which the fields are located.

In the “by-hand” expansion it simplifies the algebra to derive separate Feynman rules for A and B and combine them using the convolution theorem [13, 28]. We also follow this approach: the AB and BA factors are on different timeslices so no compression of the set of monomial factors (“entities”) contributing to the reduced vertex function can occur. Without such compression, it is computationally cheaper to calculate the Feynman rules as a convolution of the expansions of A and B . The implementation of this has been checked by comparing with the reduced vertex functions from the expansion of the full action.

Partial derivatives of the Feynman rules are computed automatically in the code as per Ref. [30]. We exploit the fact that the velocity is purely along the z -axis to write

$$\frac{\partial}{\partial \mathbf{p}^2} = \frac{1}{2p_3} \frac{\partial}{\partial p_3}. \quad (A4)$$

The total on-shell derivative is implemented as

$$\begin{aligned}
\frac{d}{d\mathbf{p}^2} &= \frac{\partial}{\partial \mathbf{p}^2} + \frac{dp_0}{d\mathbf{p}^2} \frac{\partial}{\partial p_0}, \\
\frac{dp_0}{d\mathbf{p}^2} &= \frac{i}{1 - T(\mathbf{p})} \frac{dT(\mathbf{p})}{d\mathbf{p}^2}, \quad (A5)
\end{aligned}$$

with $T(\mathbf{p}) = G_0^{-1}(0, \mathbf{p})$ coming from the bare fermion propagator.

APPENDIX B: RENORMALISING THE FERMION PROPAGATOR

In this appendix we review the one loop renormalisation of the fermion propagator. The bare fermion propagator is

$$aG_0^{-1}(p_0, \mathbf{p}) = 1 - z(1 - aT(\mathbf{p}^2)) \quad (B1)$$

where $z = e^{-iap_0}$ and $T(\mathbf{p})$ is the kinetic energy. The $\mathcal{O}(\alpha_s)$ NRQCD quark self-energy can always be written as

$$\begin{aligned}
a\Sigma(p_0, \mathbf{p}) &= A + B(p_0, \mathbf{p}) aT(\mathbf{p}) + \\
&C(p_0, \mathbf{p}) [1 - z(1 - aT(\mathbf{p}))], \quad (B2)
\end{aligned}$$

where A is a constant. The resummed propagator is

$$\begin{aligned}
aG^{-1}(p_0, \mathbf{p}) &= aG_0^{-1}(p_0, \mathbf{p}) - \alpha_s a\Sigma(p_0, \mathbf{p}) \\
&= (1 - \alpha_s(A + C)) [1 - z(1 + \alpha_s A) \times \\
&\quad (1 - aT(\mathbf{p}) [1 - \alpha_s B/z])] \\
&+ \mathcal{O}(\alpha_s^2) \quad (B3)
\end{aligned}$$

In the infrared limit of small \mathbf{p}^2 , this should be compared to the renormalised form of Eq. (B1):

$$aG^{-1} = Z_\psi^{-1} (1 - \bar{z} [1 - aT_R(\mathbf{p})]), \quad (B4)$$

with $T_R(\mathbf{p}) = \mathbf{p}^2 / (Z_M M)$. Identifying $\bar{z} = z(1 + \alpha_s A)$, the additive shift in the rest energy is

$$\begin{aligned}
a\Delta E_{\text{rest}} &= \ln(z/\bar{z}) \\
&= -\alpha_s A + \mathcal{O}(\alpha_s^2), \quad (B5)
\end{aligned}$$

and $A = a\Sigma(p_0 = 0, \mathbf{p} = \mathbf{0})$. The p_0 pole in the propagator occurs at $\bar{z} = z_0 \equiv (1 - aT_R)^{-1}$. The wavefunction renormalisation is found by Taylor expanding Eq. (B3) around this pole:

$$\begin{aligned}
Z_\psi(\mathbf{p}) &= 1 + \alpha_s \left(A + C + B aT - aT\bar{z} \frac{\partial B}{\partial \bar{z}} \right)_{\text{on-shell}} \\
&= 1 + \alpha_s \left(a\Sigma + \frac{\partial a\Sigma}{\partial (iap_0)} \right)_{\text{on-shell}} \quad (B6)
\end{aligned}$$

where the expressions are evaluated on the mass shell. As the terms in brackets are already $\mathcal{O}(\alpha_s)$, it is sufficient to identify T and T_R and evaluate them at the pole of the bare propagator $\bar{z} = (1 - aT)^{-1}$. This result is general and includes all orders in v^2 at $\mathcal{O}(g^2)$. Morningstar [28] gives the expression for Z_ψ at zeroth order in v^2 and our result agrees with his to this order.

Working on the renormalised mass shell, the mass renormalisation follows from

$$\frac{1}{2Z_M M} = \left. \frac{dT_R}{d\mathbf{p}^2} \right|_{\mathbf{p}^2=0} = \frac{1}{2M} - \alpha_s \left. \frac{d(BT)}{d\mathbf{p}^2} \right|_{\mathbf{p}^2=0}. \quad (\text{B7})$$

We note that the total differential must also be evaluated on the (bare) mass shell. From this we obtain

$$Z_M = 1 + \alpha_s 2M \left. \frac{da\Sigma}{d\mathbf{p}^2} \right|_{\mathbf{p}^2=0}. \quad (\text{B8})$$

Tadpole improvement affects ΔE_{rest} and Z_M , but not Z_ψ for NRQCD actions that are symmetric under time reversal [6]. The one-loop contributions are given in Eqs. (35, 36) of Ref. [13].

APPENDIX C: FURTHER CODE TESTS

In this appendix we describe further, non-trivial tests of our perturbative calculation that verify that our contour shifting and numerical integration techniques are correct.

1. One-loop self energy

We have calculated the renormalisation of the NRQCD propagator as per Appendix B using Feynman gauge and a gluon mass of $(a\mu)^2 = 10^{-4}$. The results are given in Table V. For comparison, we also give the results of Gulez et al. [13]. Our data agree very closely. This provides further evidence that not only are our Feynman rules correct, but also that we are combining them correctly to form diagrams and evaluating the resulting integrals correctly using VEGAS. We have also checked that the results are correctly gauge variant and that the effect of the finite gluon mass is negligible.

2. Gauge covariance and invariance

We have also looked closely at the effect of changing the gauge and infrared regulator. For these tests, we use a simpler NRQCD action with coefficients $c_i = 0$ for $i = 1 \dots 4$ and $c_5 = c_6 = 1$, as used in Ref. [10], with $n = 2$ and $aM = 2.1$. We used both the Wilson and Symanzik-improved gauge actions and set current $J_1 = 0$, which implies $I_{\text{earlobe}} = I_{\text{bubble}} = I_{\text{tadpole}} = 0$. We use three choices of gauge: Feynman gauge $\lambda = 1$,

an unnamed gauge with $\lambda = 2$ and Yennie–Fried gauge $\lambda = \frac{1}{3}$.

Firstly, $I_{\text{QCD}} - I_{\text{NRQCD}}$ should be independent both of the choice of gauge and the gluon mass. This is seen for $v = 0.03$ in Fig. 5. We note that the size of the scatter of points about a single mean value is consistent with the statistical errors assigned to the data points by VEGAS. This gives us some confidence that these errors are not being underestimated in our calculation.

Next, Z and V separately have infrared divergences that are regulated by the gluon mass, but which cancel in $Z+V$. The cancellation has already been shown by the absence of diverging behaviour at small $a\mu$ in Fig. 5.

Here we check that the individual diagrams show the correct divergence. We compare with the expectations for continuum QCD: lattice NRQCD is an effective description of this and must preserve the same infrared structure (up to possible discretisation errors of order $a\mu$).

Given the lack of overall divergence in $Z + V$, it is sufficient to concentrate on Z , which is determined to greater statistical accuracy.

The one-loop continuum expression is given in Eq. (7-44) of Ref. [22] (adding a colour factor of 4/3):

$$Z_{\text{cont}} = -\frac{1}{12\pi^2} \left(\frac{1}{\lambda} \ln \frac{\Lambda^2}{M^2} + 3 \ln \frac{\mu^2}{M^2} - \frac{1}{\lambda} \ln \frac{\mu^2}{\lambda M^2} + \frac{9}{4} \right) \quad (\text{C1})$$

The infrared divergent contribution is

$$Z_{\text{IR}} = -\frac{1}{12\pi^2} \left(3 - \frac{1}{\lambda} \right) \ln \mu^2, \quad (\text{C2})$$

which vanishes in Yennie–Fried gauge.

In Fig. 6 we plot Z with the continuum divergence removed (replacing μ by $a\mu$). There is no discernible

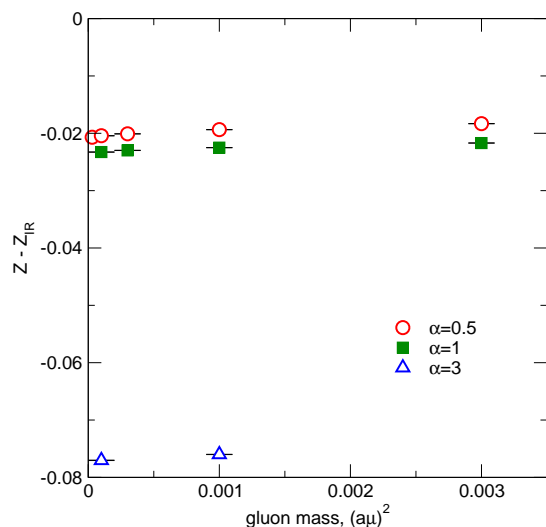


FIG. 6: $Z - Z_{\text{IR}}$ for the NRQCD action described in Appendix C 2 at $aM = 2.1$ and $v = 0.03$ using the Wilson gauge action.

TABLE V: The renormalisation of the fermion propagator, as compared to Ref. [13]. Note that an IR factor corresponding to Eq. (C2) with $(a\mu)^2 = 10^{-4}$ has been applied to the subtracted data quoted in Ref. [13] for $Z_\psi^{(1)}(\mathbf{p} = 0)$.

aM	n	$Z_\psi^{(1)}(\mathbf{p} = 0)$		$Z_M^{(1)}$		$a\Delta E_0^{(1)}$	
		Us	Ref. [13]	Us	Ref. [13]	Us	Ref. [13]
4.0	2	1.8207 (7)	1.813 (3)	0.0817 (5)	0.082 (4)	0.8390 (1)	0.850
2.8	2	1.6232 (6)	1.617 (3)	0.2350 (6)	0.235 (4)	0.7570 (10)	0.767
1.95	2	1.3494 (5)	1.344 (3)	0.4201 (8)	0.421 (4)	0.6765 (10)	0.689
1.0	4	0.4334 (7)	—	0.8285 (16)	—	0.9684 (13)	—
	6	—	0.410 (3)	—	0.859 (4)	—	0.758

divergence as $a\mu \rightarrow 0$. The slight gradient betrays a residual dependence on the gluon mass. To emphasize this, we plot the deviation $\Delta Z(a\mu) = Z(a\mu) - Z(10a\mu)$ in Fig. 7. The deviation disappears as we take $a\mu$ to zero and is a discretisation effect.

3. Current matching at $v = 0$

Finally, we have tried to verify the one-loop, $\mathcal{O}(v^0)$ annihilation current matching of Jones and Woloshyn [10]. Following the method in the main text, we get $a_0^{(1)} = -0.0225$ (3) for $(a\mu)^2 = 10^{-4}$ and -0.0228 (3) for $(a\mu)^2 = 10^{-3}$ (using $n = 2$ and $aM = 2.1$ with the Symanzik gauge action). The extrapolations to $v = 0$ are shown in Fig. 8. The statistical compatibility of the results shows that $(a\mu)^2 = 10^{-4}$ is small enough that any residual gluon mass dependence of the results is swamped by the statistical uncertainties in the VEGAS integration.

At the same parameter values, Jones and Woloshyn give $a_0^{(1)} = -0.0253$ (3) [inserting the appropriate number from Table II into their Eq. (27)]. This result broadly agrees with ours, which gives us confidence that there are no gross disagreements in our methods.

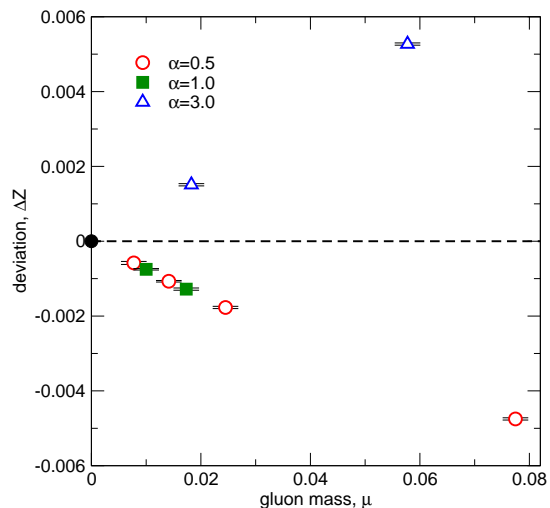


FIG. 7: ΔZ for the NRQCD action described in Appendix C 2 at $aM = 2.1$ and $v = 0.03$ using the Wilson gauge action.

There is still a small, but apparently significant deviation, which we also see at a second mass value. The stringent tests described in these Appendices were our attempt to account for this difference. As already described, we have checked our Feynman rules are correct and give the correct self energy (and derivatives). We find the correct infrared divergences and Lorentz invariance. We have gauge invariance and independence on the gluon mass regulator. We have also checked that the statistical errors quoted by VEGAS are not underestimated. In the light of these, we feel confident that our calculation is correct.

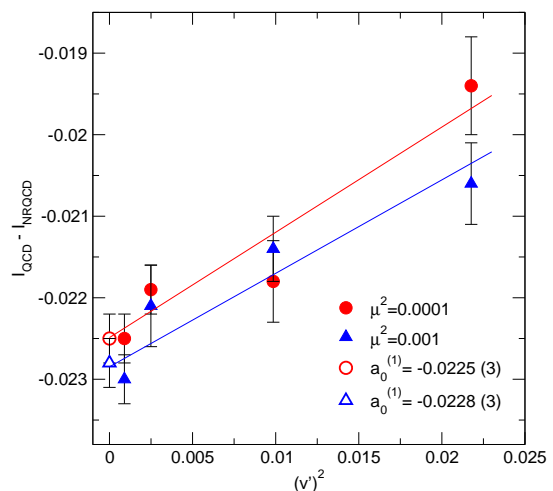


FIG. 8: Determination of $a_0^{(1)}$ for the NRQCD action described in Appendix C 2 at $aM = 2.1$ and $v = 0.03$ using the Wilson gauge action.

-
- [1] J. J. Aubert *et al.*, Phys. Rev. Lett. **33**, 1404 (1974).
- [2] J. E. Augustin *et al.*, Phys. Rev. Lett. **33**, 1406 (1974).
- [3] C. E. Carlson and R. Suaya, Phys. Rev. Lett. **39**, 908 (1977).
- [4] S. W. Herb *et al.*, Phys. Rev. Lett. **39**, 252 (1977).
- [5] W. E. Caswell and G. P. Lepage, Phys. Lett. **B167**, 437 (1986).
- [6] G. P. Lepage, L. Magnea, C. Nakhleh, U. Magnea and K. Hornbostel, Phys. Rev. **D46**, 4052 (1992), [hep-lat/9205007].
- [7] C. J. Morningstar and J. Shigemitsu, Phys. Rev. **D57**, 6741 (1998), [hep-lat/9712016].
- [8] C. J. Morningstar and J. Shigemitsu, Phys. Rev. **D59**, 094504 (1999), [hep-lat/9810047].
- [9] G. T. Bodwin and A. Petrelli, Phys. Rev. **D66**, 094011 (2002), [hep-ph/0205210].
- [10] B. D. Jones and R. M. Woloshyn, Phys. Rev. **D60**, 014502 (1999), [hep-lat/9812008].
- [11] G. T. Bodwin, D. K. Sinclair and S. Kim, Phys. Rev. **D65**, 054504 (2002).
- [12] HPQCD, A. Gray *et al.*, Phys. Rev. **D72**, 094507 (2005), [hep-lat/0507013].
- [13] E. Gulez, J. Shigemitsu and M. Wingate, Phys. Rev. **D69**, 074501 (2004), [hep-lat/0312017].
- [14] A. Hart, G. M. von Hippel and R. R. Horgan, PoS **LAT2006**, 098 (2006), [hep-lat/0609002]. ”
- [15] E. Braaten and S. Fleming, Phys. Rev. **D52**, 181 (1995).
- [16] G. Lepage, Private communication.
- [17] P. Weisz, Private communication.
- [18] M. H. L. Pryce, Proc. Roy. Soc. Lond. **A195**, 62 (1948).
- [19] S. Tani, Soryushiron Kenyu **1**, 15 (1949), (in Japanese).
- [20] S. Tani, Prog. Theor. Phys. **6**, 267 (1950).
- [21] L. L. Foldy and S. A. Wouthuysen, Phys. Rev. **78**, 29 (1950).
- [22] C. Itzykson and J.-B. Zuber, *Quantum Field Theory*, International ed. (McGraw-Hill, 1985).
- [23] R. Karplus and N. M. Kroll, Phys. Rev. **77**, 536 (1950).
- [24] C. Davies, Private communication, 2006.
- [25] B. A. Thacker and G. P. Lepage, Phys. Rev. **D43**, 196 (1991).
- [26] C. T. H. Davies and B. A. Thacker, Phys. Rev. **D45**, 915 (1992).
- [27] W. H. Press *et al.*, *Numerical Recipes in FORTRAN*, Second ed. (Cambridge University Press, 1992).
- [28] C. J. Morningstar, Phys. Rev. **D48**, 2265 (1993), [hep-lat/9301005].
- [29] M. Wingate, J. Shigemitsu, C. T. H. Davies, G. P. Lepage and H. D. Trottier, Phys. Rev. **D67**, 054505 (2003), [hep-lat/0211014].
- [30] A. Hart, G. M. von Hippel, R. R. Horgan and L. C. Storoni, J. Comput. Phys. **209**, 340 (2005), [hep-lat/0411026].
- [31] I. T. Drummond, A. Hart, R. R. Horgan and L. C. Storoni, Phys. Rev. **D66**, 094509 (2002), [hep-lat/0208010].
- [32] G. P. Lepage and P. B. Mackenzie, Phys. Rev. **D48**, 2250 (1993), [hep-lat/9209022].
- [33] M. A. Nobes, H. D. Trottier, G. P. Lepage and Q. Mason, Nucl. Phys. Proc. Suppl. **106**, 838 (2002), [hep-lat/0110051].
- [34] G. P. Lepage, J. Comput. Phys. **27**, 192 (1978).
- [35] G. P. Lepage, Vegas: An adaptive multidimensional integration program, Cornell preprint CLNS-80/447, March 1980.
- [36] M. Luscher and P. Weisz, Nucl. Phys. **B266**, 309 (1986).
- [37] H. D. Trottier, N. H. Shakespeare, G. P. Lepage and P. B. Mackenzie, Phys. Rev. **D65**, 094502 (2002), [hep-lat/0111028].
- [38] I. T. Drummond, A. Hart, R. R. Horgan and L. C. Storoni, Nucl. Phys. Proc. Suppl. **119**, 470 (2003), [hep-lat/0209130].
- [39] I. T. Drummond, A. Hart, R. R. Horgan and L. C. Storoni, Phys. Rev. **D68**, 057501 (2003), [hep-lat/0307010].
- [40] A. Hart, R. R. Horgan and L. C. Storoni, Phys. Rev. **D70**, 034501 (2004), [hep-lat/0402033].